Hindawi
Journal of Advanced Transportation
Volume 2022, Article ID 5869101, 12 pages
https://doi.org/10.1155/2022/5869101

Research Article

An Improved Runway Operation Capacity Model for V-Open Multirunway Airports in China

Zhiyuan Shen,[1] **Xinyu Xu**,[1] **Yong He**,[2] **YongGang Yan**,[3] **Lin Zhou**,[4] **and Yingying Hu**[1]

[1]*College of Civil Aviation, Nanjing University of Aeronautics and Astronautics, Nanjing, China*
[2]*East China Air Traffic Management Bureau, Civil Aviation Administration of China, Shanghai, China*
[3]*Central Air Traffic Management Committee, Beijing, China*
[4]*East China Air Traffic Management Bureau at Zhejiang Sub-Bureau, Civil Aviation Administration of China, Hangzhou, China*

Correspondence should be addressed to Zhiyuan Shen; shenzy@nuaa.edu.cn

Received 24 May 2022; Revised 2 August 2022; Accepted 30 September 2022; Published 12 October 2022

Academic Editor: Shao-Wu Cheng

Diverging runways are receiving considerable attention as replacements for parallel runways when constructing three or more runways in China. This has been prompted by the limitations associated with a single-direction airspace and associated regulations when using parallel runways. However, the operating efficiency of diverging runways is still greatly constrained by the separation standard for departing aircraft in CCAR-93TM-R5 and Decree of CAAC NO.123. To address these problems, an improved runway operation capacity model for a V-open multirunway airport is proposed to reduce the separation standard based on the equivalent lateral separation operation (ELSO) standard. A collision risk module is first proposed to assess the feasibility and safety of the proposed policy. Also, a novel runway capacity model for V-open multiple runways is then built to improve the operating efficiency for diverging runway. A series of comparative experiments based on actual flight data from Chengdu Tianfu International Airport demonstrated that reducing the divergence angle from 15° to 10° improved the runway operation capacity by about 8% based on the proposed improved policy. These research results could play a major role in facilitating appropriate amendments to the associated CAAC operation regulations.

1. Introduction

The International Air Transport Association (IATA) has predicted that China will become the largest civil aviation market in the world by around 2025 and involve the flow of 1.6 billion passengers by around 2037 [1]. Then, there is no doubt that COVID-19 significantly impacted civil aviation market and considered as the main factor in much recent studies [2]. Research studies on runway capacity estimation usually focus on the maximum of capacity in peak hour or one day. So, airline and airport pay more attention to theoretical maximum flight number under the priority of operation safety. By reducing the impact of the diverging angle, the departure separation can be decreased. Thereby, the numbers of airport flights permitted to taking-off and landing at peak hour increase. The ticket price at peak hour is usually higher than those at other time. Consequently, it leads to a higher airline revenue.

In the past, large airports at China tended to build additional parallel runways to improve their operation capacity. However, it has been difficult to reach estimated maximum operation capacities due to limitations associated with a single-direction airspace and its associated regulations. The diverging runway has advantages of low building cost and flexible operation procedures; therefore, it is the preferred choice for configuration of large domestic hub airports. It has led to diverging runways being considered for replacing parallel runways when constructing three or more runways in China, such as at Beijing Daxing International Airport (ZBAD) and Chengdu Tianfu International Airport (ZUTF). While configuring runways in different directions facilitates the flexible utilization of airport airspace and

operation procedures, such diverging runways have mainly been used for aircraft takeoffs [3].

However, the departure efficiency for diverging runways is still greatly affected by the separation standard for departing aircraft in CCAR-93TM-R5 [4] and Decree of CAAC NO.123 [5]. Specifically, aircraft departing simultaneously from parallel or diverging runways need to comply with the separation standard that their takeoff courses diverge by 15° or more immediately after departure. The initial purpose of implementing diverging departures is to improve the operating efficiency and reduce flight delays [6]. However, numerous studies have shown that the strict separation standard greatly restricts the use of the available airspace, especially for multiple runways and diverging runways [7, 8]. For example, a larger diverging airspace is needed when applying the separation standard to three parallel runways, and separated departure flight paths could overlap the diverging runways to result in increased waiting time for aircraft departures or reducing the takeoff runway distance, resulting in a decreased departure capacity. Therefore, many studies have attempted to reduce the divergence angle while still conforming to safety standards [9, 10].

The recent rapid development and application of performance based on navigation (PBN) has significantly improved navigation precision in the terminal area. A novel concept of the equivalent lateral separation operation (ELSO) standard [11] was proposed, which is able to reduce divergence angles while maintaining established minimum lateral spacing between departure paths. A series of related theorical and practical evaluation experiments were conducted at Atlanta Airport over a 1-year period in 2011 [12]. The Federal Aviation Administration (FAA) finally approved for the divergence angle to be reduced to 10° at Atlanta Airport based on the safety of the experimental results, which facilitated the development of a new departure procedure. Nowadays, any airport in the USA can operate with the standard 10° divergence angle when both aircraft are flying RNAV (area navigation) standard instrument departures (SID) from parallel runways according to the policy in FAAO.7110.65W [13].

All of the international airports in China have been designed and operated under RNAV SID procedures, and more runways are planned to be built in order to meet the increasing number of flights at the busiest Chinese airports (e.g., Shanghai Pudong, Hangzhou Xiaoshan, and Yunnan Changshui), including to stimulate the economy affected by COVID-19 with greater infrastructure investment [14–16]. Reducing delays and improving operation efficiency are two important steps to reduce the impact of COVID-19 on the aviation industry. However, the superiority of the higher navigation precision of RNAV has not been performed to improve the operating efficiency for the applicable standard and additional runways [17, 18]. Most importantly, the existing separation standard, including the minimum requirement for a 15° divergence angle between independent parallel departure operations, significantly constrains the potential of multirunway operations [19].

In accordance with the development strategies of the CAAC and the Central Military Commission (CMC) of ATC that pertain to higher flight punctuality rates and better civil airspace planning [20], based on the actual aircraft departure path data from ZUTF parallel runways, we proposed modifying the regulations associated with the separation standard by referring to the ELSO standard. We further proposed a capacity estimation model for V-open multiple runways and tested the operating efficiency of the proposed new separation standard relative to the conventional one. Specifically, taking ZUTF as an example, two main modules are developed to test the assumption: (1) the collision risk module based on ELSO for assessing the feasibility and safety of the proposed policy, and (2) the V-open multirunway capacity module for measuring the increases in runway capacity. This study provides theoretical support and reference data for the development of future regulations to reduce the divergence angle standard and the operation procedure of V-open runways. All terminology used in this paper is listed in Table 1.

The remainder of this paper is organized as follows: Section 2 describes the basic theory of V-open runway configuration and ELSO, Section 3 details the proposed collision risk module and V-open multirunway capacity module, Section 4 reports on the theoretical analyses and experimental simulations performed to test our proposed framework, and Section 5 summarizes the obtained findings.

2. Basic Theory

The current divergence requirements for departing aircraft are defined in CCAR-93TM-R5 and Decree of CAAC NO.123. There are three key rules involved in separating aircraft departing from the same runway or parallel runways based on using either conventional SID or RNAV SID. In all cases, aircraft must establish radar identification within 1 mile of the end of the takeoff runway and travel along courses that diverge by 15° or more immediately after departure.

2.1. Layout of V-Open Runways. The layout of the runways at two airports (ZBAD and ZUTF) with diverging runways served as the research model of V-open runways in this study. As illustrated in Figure 1, including three runways totally in our study scene, two runways are parallel, and the other runway is V-open with the parallel runways. For parallel runways, we try to use ELSO to reduce the angle of course divergence for improving the efficiency of airspace usage. For the V-open runway, the main effort is to reduce the coverage impact of the parallel runway departure courses on the third runway. The diverging runway in the figure is used only for aircraft departures toward the east direction. One departure course coincides with the runway centerline extension; another one diverged by alpha angle. In this case, pilots are rather easier to master departing course whatever runway is used. On the other hand, the location of the runway direction is significantly affected by the surrounding terrain, so departure courses along the extension line of the runway centerline could minimize obstacle restrictions. Therefore, there is no need to simultaneously consider

Table 1: List of terminology used in this paper.

Terminology	Referred to
ELSO	Equivalent lateral separation operation
CAAC	Civil Aviation Administration of China
IATA	International Air Transport Association
ZBAD	Beijing Daxing International Airport
ZUTF	Chengdu Tianfu International Airport
PBN	Performance based on navigation
FAA	Federal Aviation Administration
RNAV	Area navigation
SID	Standard instrument departures
CMC	Central Military Commission

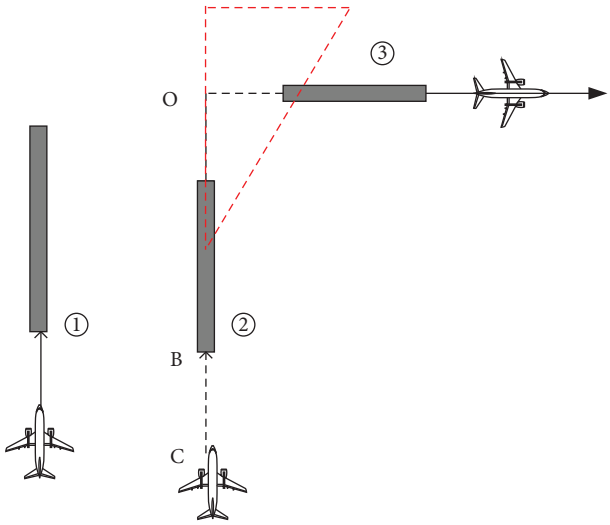

Figure 1: Layout of a V-open runway.

mutual diversion and considering one runway's trajectory divergence could better estimate the runway.

In accordance with the regulations in CCAR-93TM-R5, aircraft can depart from parallel runways simultaneously when the centerlines of the parallel runways are separated by at least 760 m and the courses of the aircraft diverge by 15° or more immediately after departure. In terms of approach operations, correlated parallel approaches and independent parallel approaches are authorized for minimum parallel runway spacing of 915 m and 1035 m, respectively.

The departure course relative to the runway centerline might cover the takeoff zone of the diverging runway in Figure 1. In other words, the departure interval for diverging runways is highly dependent on the time separation between aircraft flying over the intersection zone. There is no doubt that this situation will adversely affect the airport operating efficiency and runway capacity [21]. The concept of ELSO is introduced to solve this problem in this study.

2.2. Principle of ELSO. ELSO was proposed to meet the minimum spacing of the general divergence standard defined in CCAR-93TM-R5. In other words, the divergence angle can be reduced as long as the established minimum lateral spacing between departure paths is maintained. After a 1-year safety evaluation experiment was conducted at Atlanta Airport in 2011, the FAA authorized that the course divergence angle could be reduced to 10° when both aircraft are departing from parallel runways and are flying RNAV SID.

For the independent parallel departure operation, the general standard defines that the minimum spacing between parallel runways ($r_{\min}$) should be 760 m and that the departure-course divergence ($\alpha_{\min}$) should be a minimum of 15°. Figure 2 illustrates some key parameters of the general departure operation. In the figure, dashed lines represent the nominal departure path and the distance (d) from the runway end will determine nominal spacing ($n(d)$) between the nominal departure path, which can be obtained as follows: [22]

$$n(d) = r_{\min} + d \times \tan(\alpha_{\min}). \tag{1}$$

The actual path deviation due to various factors such as the wind direction is also illustrated in Figure 2. We can assume that the resulting width of the departure path can be estimated by single or multiple standard deviations (σ) of the related dispersion distribution. Hence, $\sigma_{\mathrm{STO},C}$ represents the track width of the conventional straight departure procedure along the centerline of the runway, and $\sigma_{\mathrm{DIV},C}$ indicates the track width of the diverging conventional departure procedure. The lateral spacing of the diverging departure path is given as follows:

$$s(d) = r_{\min} + d \times \tan\left(\alpha_{\min} - \sigma_{\mathrm{DIV},C}\right) - d \times \tan\left(\sigma_{\mathrm{STO},C}\right). \tag{2}$$

Therefore, distance $s(d)$ can be regarded as the minimum lateral spacing between actual departure flight paths under the conventional divergence standard and serves as the reference distance when using the ELSO standard.

When parallel runways are separated by more than 760 m, lateral spacing requirement $s(d)$ can also be achieved for a smaller divergence angle, as shown in Figure 3. In the figure, $\sigma_{\mathrm{STO},R}$ indicates the width of the RNAV departure path following the extended centerline, and the width of the RNAV departure path whose centerline is angled relative to the runway centerline is $\sigma_{\mathrm{DIV},R}$.

Given reference distance $s(d)$ and staggered distance t at the end of the runway, the runway distance can be expressed as follows:

$$r = s(d) + d \cdot \tan\left(\sigma_{\mathrm{STO},R}(d)\right) - (d+t)\tan\left(\beta - \sigma_{\mathrm{DIV},R}(d+t)\right), \tag{3}$$

where $\sigma_{\mathrm{STO},R}(d)$ and $\sigma_{\mathrm{DIV},R}(d+t)$ represent the actual track divergence characteristics of RNAV straight-line departure and offset departure, respectively. Therefore, based on the specific runway configuration, equivalent divergence angle β that can implement independent parallel departures under the ELSO standard is as follows:

$$\beta = \arctan\left\{\left(\frac{1}{d+t}\right) \cdot \left(s(d) - r + d \cdot \tan\left(\sigma_{\mathrm{STO},R}(d)\right)\right\}\right. \\ \left. + \sigma_{\mathrm{DIV},R}(d+t). \right. \tag{4}$$

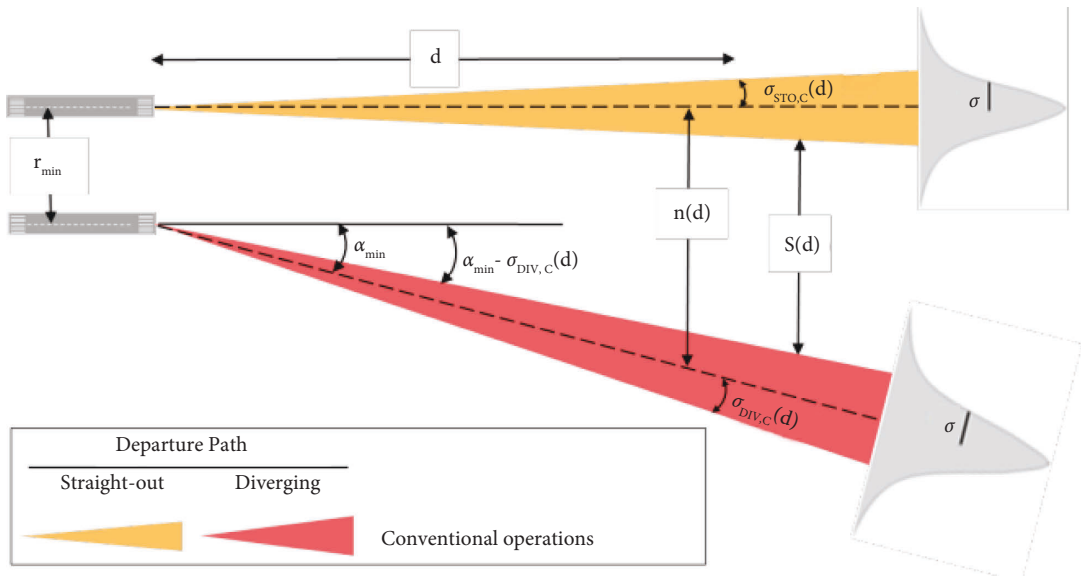

Figure 2: Conventional departure path and associated parameters.

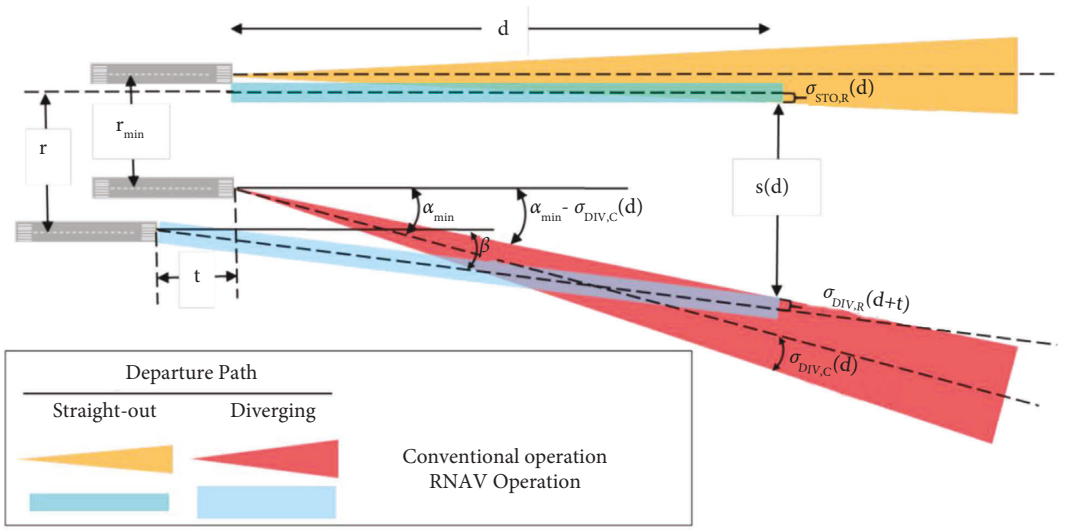

Figure 3: Improved departure path based on ELSO.

Equivalent divergence angle β can ensure that the departure path distance at the end of the runway (d) is the same as or even greater than the reference distance. If the nominal departure path fails to establish a lateral separation of d nautical miles from the end of the runway, the ELSO divergence standard will assume that the departure will be implemented with the traditional 15° divergence angle after this distance.

3. Proposed Modules

A collision risk model was proposed to quantitatively evaluate safety when the divergence angle is reduced based on ELSO. The minimum divergence angle can also be obtained under the safety requirement. In order to further assess the benefits of the new standard, we determined the operating efficiency of a V-open multirunway capacity model.

3.1. Collision Risk Model. The collision risk model mainly considered the path deviation of the actual flight caused by the precision of navigation equipment, which is greatly affected by the aircraft speed. We can assume that both the navigation error and speed error conform to a Gaussian distribution and are given as follows:

$$\varepsilon_{ny} \sim N\left(\mu_n, \sigma_n^2\right), \tag{5}$$

$$\varepsilon_{ay} \sim N\left(\frac{1}{2}\mu_a t^2, \frac{1}{4}\sigma_a^2 t^4\right), \tag{6}$$

where μ_n and μ_a indicate the mean values and σ_n and σ_a are the standard deviations. Subscripts ny and ay denote the aircraft lateral deviation caused by two factors. The lateral collision risk can be computed using equations (7) to (10):

$$\begin{aligned} &\varepsilon_y \sim N\left(\mu_y, \sigma_y^2\right) \\ &\mu_y = \mu_n + \frac{1}{2}\mu_a t^2, \sigma_y^2 = \sigma_n^2 + \frac{1}{4}\sigma_a^2 t^4 \end{aligned}, \tag{7}$$

where ε_y denotes the distribution of the lateral deviation. The actual lateral distance between simultaneously departing aircraft is given as follows:

$$\begin{aligned} D_y'(t) &= L_{2y}'(t) - L_{1y}'(t) = D_y(t) + \left(\varepsilon_{2y} - \varepsilon_{1y}\right) \\ &\sim N\left(D_y(t) + \mu_{2y} - \mu_{1y}, \sigma_{2y}^2 + \sigma_{1y}^2\right) \\ L_{1y}'(t) &= L_{1y}(t) + \varepsilon_{1y}, L_{2y}'(t) = L_{2y}(t) + \varepsilon_{2y} \end{aligned}, \tag{8}$$

where $L_{1y}'(t)$ and $L_{2y}'(t)$ represent the actual path positions of two different aircraft. The probability density function for the lateral direction can be expressed as follows:

$$f(y) = \frac{1}{\sqrt{2\pi\left(\sigma_{2y}^2 + \sigma_{1y}^2\right)}} \exp\left(-\frac{\left(y - \left(D_y(t) + \mu_{2y} - \mu_{1y}\right)\right)^2}{2\left(\sigma_{2y}^2 + \sigma_{1y}^2\right)}\right). \tag{9}$$

The probability density function of the actual distance between the two aircraft is integrated to obtain the lateral collision risk:

$$P_y = p\left\{y_1 < D_y'(t) < y_2\right\} = \int_{y_1}^{y_2} f(y)dy, \tag{10}$$

where y_1 and y_2 represent the minimum and maximum separations between the aircraft, respectively, and can be calculated from the aircraft wing spans. Similarly, the probability density functions in the vertical and horizontal directions are given as follows:

$$f(x) = \frac{1}{\sqrt{2\pi\left(\sigma_{2x}^2 + \sigma_{1x}^2\right)}} \exp\left(-\frac{\left(x - \left(D_x(t) + \mu_{2x} - \mu_{1x}\right)\right)^2}{2\left(\sigma_{2x}^2 + \sigma_{1x}^2\right)}\right), \tag{11}$$

$$f(z) = \frac{1}{\sqrt{2\pi\left(\sigma_{2z}^2 + \sigma_{1z}^2\right)}} \exp\left(-\frac{\left(z - \left(D_z(t) + \mu_{2z} - \mu_{1z}\right)\right)^2}{2\left(\sigma_{2z}^2 + \sigma_{1z}^2\right)}\right), \tag{12}$$

Finally, the collision risk model is obtained as follows:

$$P = \int_{x_1}^{x_2} f(x)dx \int_{y_1}^{y_2} f(y)dy \int_{z_1}^{z_2} f(z)dz. \tag{13}$$

3.2. V-Open Multirunway Capacity Model. Wake turbulence was one of the main factors influencing the design of the V-open multirunway capacity model [23, 24]. At domestic hub airports, the number of medium aircraft accounts for 99% and heavy aircraft accounts for 1% at Chinese domestic hub airports. Therefore, in most cases, it is necessary to consider the wake impact for medium aircraft following heavy or medium aircraft, and detailed wake interval and accounts of different categories are shown in Table 2. Mainly, the wake generated from taking-off aircraft on the diverging runway affects the operation of departing aircraft on parallel runways and vice versa. A typical layout of V-open multiple runways is illustrated in Figure 1, in which there are two parallel runways and one diverging runway. There are generally two approach operations for parallel runways depending on whether or not they have different widths: independent parallel approach and correlated parallel approach [25]. Small airports in China currently use independent parallel approaches due to the high requirements for equipment and working skills. However, another diverging path of 30° for aircraft to safely go around also needs to be considered [26]. Therefore, the capacity evaluation model was proposed here based only on the correlated parallel approach.

An operation schematic diagram of parallel runways using the correlated parallel-approach-independent parallel departure mode is shown in Figure 4. Both runways are used for aircraft arrivals and departures. Aircraft arrive and depart on each runway independently of each other. However, in order to ensure the safe operation of aircraft, the aircraft must land in the same direction on Runways 1 and 2. A safe distance needs to be maintained between aircraft on the parallel runway approaches (δ_a).

Assuming that the distance between the two runways is D, as shown in Figure 4, the distance between two successively approaching aircraft on Runway 1 is the following:

$$l_{\min} = 2\sqrt{\left(\delta_a\right)^2 - D^2}. \tag{14}$$

Then, the time interval between two successively approaching aircraft a and aircraft c on Runway 1 is as follows:

$$t_{\min} = \max\left(\frac{l_{\min}}{v}\right). \tag{15}$$

The controller can use the insertion method to arrange for aircraft b to land on Runway 2 between aircraft a and aircraft c, but the time interval between aircraft a and aircraft c must be consistent with the following formula [27]:

$$T_{ac} + B_{ac} \geq t_{\min}. \tag{16}$$

The operation sequence diagram of three runways for Runways 1 and 2 using related parallel-approach-independent parallel departure procedures is shown in Figure 5. Assuming that approaching aircraft a on Runway 1 arrives at the runway threshold at 00:00, then within the interval between aircraft a and aircraft c, the departing aircraft can be released on Runway 1 or the approaching aircraft can be arranged to land on Runway 2. During time gap G_2 of the continuous-approach aircraft on Runway 2, the departing aircraft can continue to be released, but the controller can also release the departing

Table 2: Wake influence parameters.

Category	SH-SH	SH-SM	SM-SH	SM-SM
Wake interval	8 km	6 km	10 km	6 km
Accounts	4%	16%	16%	64%

Remarks: SH/SM denotes heavy and medium aircraft separately.

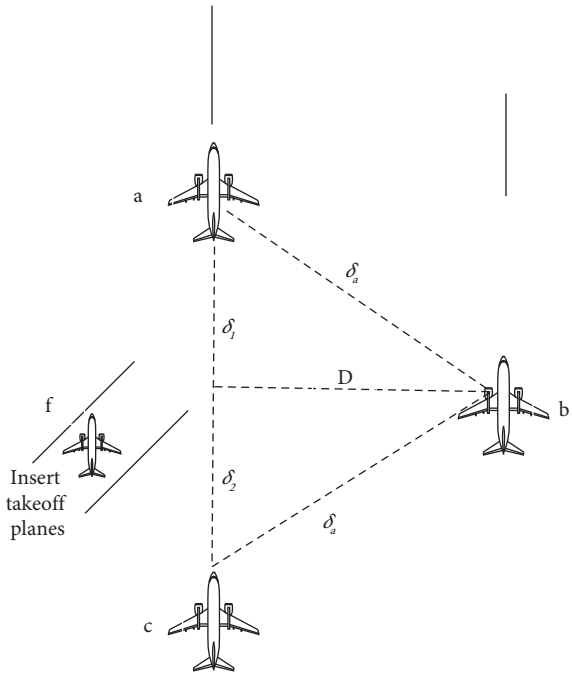

Figure 4: Parallel approach operations.

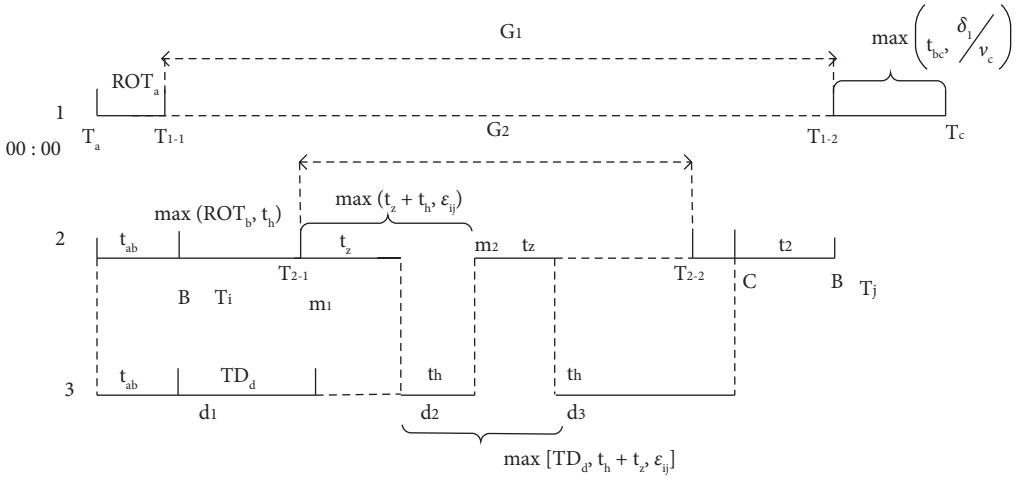

Figure 5: Time sequence model of V-open three-runway operation.

aircraft on Runway 3 after the departing aircraft on Runway 2 has been released for time t_z.

Time interval G_1 between two consecutively approaching aircraft on Runway 1 is as follows:

$$G_1 = T_{1-2} - T_{1-1} = T_{ac} + B_{ac} - ROT_a - \max(t_{bc}, t_{\min}). \tag{17}$$

When $G_1 > 0$ (i.e., when the following conditions are satisfied), n departing aircraft can be inserted in gap G_1:

$$E[T_{ac} + B_{ac}] \geq E[ROT_a] + (n-1) \cdot E(\varepsilon_{ac}) + E[\max(t_{bc}, t_{\min})] + E(\tau). \tag{18}$$

Then, the entry and exit capacities of Runway 1 are as follows:

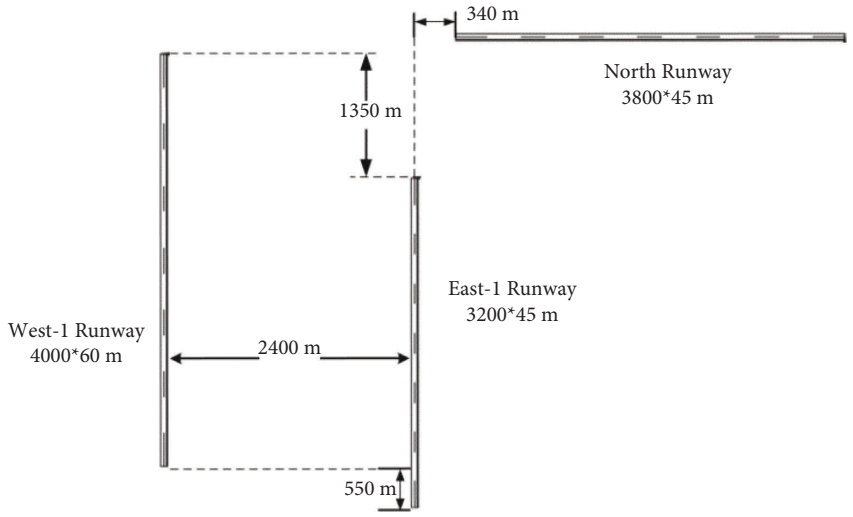

Figure 6: V-open runway layout at ZUTF.

$$C_{1-\text{arrival}} = \frac{3600}{E\left[T_{ac} + B_{ac}\right]}, \tag{19}$$

$$C_{1-\text{departure}} = \sum_{i=1}^{n}\sum_{j=1}^{n} TG_1 \cdot P_{ij} \cdot n_{ij}, \tag{20}$$

where TG_1 is the total number of clearances on Runway 1 within 1 h and n_{ij} is the number of departing aircraft that can be released between two adjacent approaching aircraft N/M on Runway 1.

Time interval G_2 between two successively approaching aircraft on Runway 2 is as follows:

$$G_2 = T_{1-2} - T_{1-1} = T_{ij} + B_{ij} - \max\left(ROT_b, t_h\right) - \max\left(t_2, \frac{\delta}{v_j}\right). \tag{21}$$

When the following conditions are met, k departing aircraft can be inserted in gap G_2:

$$E\left[T_{ij} + B_{ij}\right] \geq E\left[\max\left(ROT_b, t_h\right)\right] + (n-1) \cdot E\left[\max\left(t_z + t_h, \varepsilon_{ij}\right)\right] + E\left[\max\left(t_2, \frac{\delta}{v_j}\right)\right] + E(\tau). \tag{22}$$

Then, the entry and exit capacities of Runway 2 are as follows:

$$C_{2-\text{arrival}} = \sum_{i=1}^{n}\sum_{j=1}^{n}\sum_{x}^{TG_1} \frac{G_x}{E\left[T_{ij} + B_{ij}\right]}, \tag{23}$$

$$C_{2-\text{departure}} = \sum_{i=1}^{n}\sum_{j=1}^{n} TG_2 \cdot P_{ij} \cdot k_{ij}, \tag{24}$$

where G_x is the time interval between the first successive approach aircraft on Runway 1, TG_1 and TG_2 are the total numbers of clearances on Runways 1 and 2, respectively, within 1 h, and k_{ij} is the number of takeoff and departing aircraft that can be inserted in the time interval between two consecutively arriving aircraft i and j on Runway 2.

In gap G_2 of Runway 2, assuming that Runway 3 can release m aircraft, according to the operation sequence diagram, the following equation can be derived:

$$\left(T_j - t_2\right) - T_{2-1} \geq (m-1) \cdot \max\left[TD_d, t_z + t_h, \varepsilon_{ij}\right] + \tau, \tag{25}$$

Therefore, the departure capacity of Runway 3 is as follows:

$$C_{3-\text{departure}} = \sum_{i=1}^{n}\sum_{j=1}^{n} TG_2 \cdot P_{ij} \cdot m_{ij}, \tag{26}$$

where m_{ij} is the number of takeoff and departing aircraft that can be inserted in the interval between two consecutively arriving aircraft i and j on Runway 2.

4. Experiments and Analysis

This section describes associated experiments and data analysis for the runway layout at ZUTF. As presented in Figure 6, this airport has two parallel runways separated by 2400 m and one diverging runway whose centerline is angled at 90°. The West Runway and East Runway are used for northbound departures and landings, and the North Runway is only used for eastward departures. The collision risk for a reduced divergence angle is evaluated to determine whether it satisfies the minimum requirement. The increase in the runway capacity is determined by a theoretical analysis and further tested using simulation experiments.

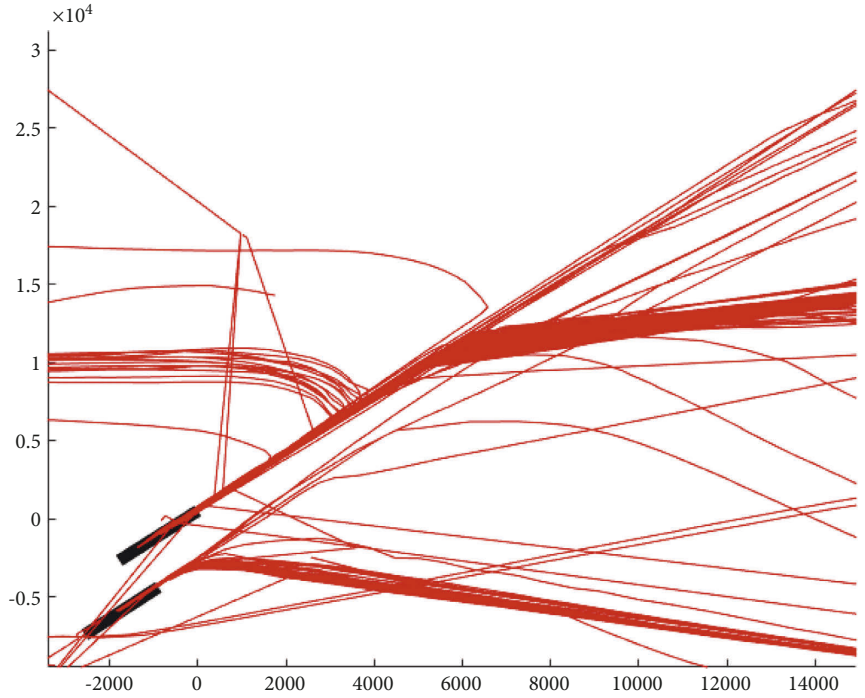

Figure 7: Analysis of actual departure paths at ZUTF.

Table 3: Performance parameters of different aircraft.

Aircraft type	Length of fuselage (m)	Wing span (m)	Height of fuselage (m)	Final approach speed (km/h)	Runway threshold speed (km/h)	Takeoff speed (km/h)	Normal cruising speed (km/h)
Heavy	68.5	64.3	12.55	296	287	293	916
Medium	39.5	34.31	9.7	258	249	269	839
Light	16.55	16.97	4.86	213	204	189	333

4.1. Analysis of Collision Risk. The reference distance from the runway end is generally set as 10 nm (18.6 km) to calculate the reference spacing when applying the ELSO standard. Then, by analyzing the actual departure path at ZUTF (see Figure 7), which contains 998 flight data all departing from parallel runways on December 14 and 15, 2021, the path variance angle is obtained as $\sigma_{\mathrm{STO,C}} = 0.4^{\circ}$ and $\sigma_{\mathrm{DIV,C}} = 0.6^{\circ}$. In this case, minimum lateral spacing $s(d)$ can be easily obtained using equation (2) as the conventional divergence standard.

The width of the parallel runways at ZUTF is 2400 m and the runways are staggered by 1350 m. In this case, equation (4) can be used to evaluate the effect of reducing the divergence angle to 10° according to the ELSO standard.

Experiments on the collision risk were performed for the proposed risk evaluation model using MATLAB software (version 2020). The experimental parameters for aircraft departing from the parallel runways with a separation path angle of 10° and three types of aircraft (heavy, medium, and light) are listed in Table 3.

When the crosswind speed is 6 kt, the aircraft wake moves at 15 ft/s. The time needed from aircraft takeoff to the first navigation point during the departure procedure is about 120 s. Research has shown that the lateral movement distance of the wake at a wind speed of 6 kt is 640 m.

Table 4: Collision risk calculation parameters.

Parameter	Value
μ_n	0
σ_n	3
μ_a	0
σ_a	1.27
R	2400
σ_g	50
$D_z(t)$	300

The parameters of the collision risk model are listed in Table 4. The upper limit of the collision probability integration interval is given by the following equation:

$$y_1 = \frac{\left(\lambda_{1y} + \lambda_{2y}\right)}{2}. \tag{27}$$

The lower limits of the collision probability integration interval in the lateral, longitudinal, and vertical directions are given by the following equation:

$$\begin{cases} y_2 = \min\left(y_1 + 640, 2400 - y_1\right) \\ x_2 = x_1 + \left(5 + \overline{v}_{\mathrm{former.flight}}\right) \times 120 \\ z_2 = \min\{z_1 + (2+2) \times 120, 300 - z_1\} \end{cases}. \tag{28}$$

Table 5: Probabilities of collision risk with different divergence angles.

Divergence angle (degree)	Aircraft type	Side collision risk	Longitudinal collision risk	Vertical collision risk	Total collision risk
14	Heavy-heavy	7.4268×10^{-6}	2.7528×10^{-10}	1.6612×10^{-5}	3.3872×10^{-20}
	Heavy-medium	7.3578×10^{-6}	2.7415×10^{-10}	1.6844×10^{-5}	3.3833×10^{-20}
	Medium-medium	7.1581×10^{-6}	2.6924×10^{-10}	1.5512×10^{-5}	2.9811×10^{-20}
13	Heavy-heavy	9.6952×10^{-6}	2.6852×10^{-10}	1.6512×10^{-5}	4.2849×10^{-20}
	Heavy-medium	9.5586×10^{-6}	2.6964×10^{-10}	1.6300×10^{-5}	4.1873×10^{-20}
	Medium-medium	9.3254×10^{-6}	2.5368×10^{-10}	1.5946×10^{-5}	3.7491×10^{-20}
12	Heavy-heavy	2.7485×10^{-5}	2.7256×10^{-10}	1.6102×10^{-5}	1.1736×10^{-20}
	Heavy-medium	2.5263×10^{-5}	2.7415×10^{-10}	1.5968×10^{-5}	1.0732×10^{-20}
	Medium-medium	2.1452×10^{-5}	2.7238×10^{-10}	1.5317×10^{-5}	8.6751×10^{-19}
11	Heavy-heavy	4.5685×10^{-5}	2.6852×10^{-10}	1.6012×10^{-5}	1.9553×10^{-19}
	Heavy-medium	4.3947×10^{-5}	2.6732×10^{-10}	1.5858×10^{-5}	1.7664×10^{-19}
	Medium-medium	4.0359×10^{-5}	2.5845×10^{-10}	1.5577×10^{-5}	1.6075×10^{-19}
10	Heavy-heavy	7.3195×10^{-5}	2.8601×10^{-10}	1.6302×10^{-5}	3.4127×10^{-19}
	Heavy-medium	7.2873×10^{-5}	2.8586×10^{-10}	1.6400×10^{-5}	3.4163×10^{-19}
	Medium-medium	7.2647×10^{-5}	2.7985×10^{-10}	1.32852×10^{-5}	2.7009×10^{-19}

Table 6: Runway capacity calculation parameters.

Parameter	Value
DD interval	100 s
DA interval	180 s
AA interval	100 s
Minimum distance between landing aircraft and entrance	95 s
Average runway occupation time of approaching aircraft (ROT_i).	50 s
Average runway occupation time of departing aircraft (TD_i).	55 s
Final approach speed of heavy aircraft	300 km/h
Final approach speed of medium aircraft	270 km/h
$\sigma_{V\text{heavy}}$	0.14 (km/h)
$\sigma_{V\text{medium}}$	0.14 (km/h)

Table 7: Calculation results for runway capacity.

Runway capacity (aircraft/h)	Related parallel-approach-independent parallel departure	
	Existing	Optimized
West Runway	32	32
East Runway	26	29
North Runway	30	33
Total capacity	88	94

According to the collision risk model based on the calculation parameters, the collision risk of departing aircraft on the parallel West Runway and East Runway can be calculated as presented in Table 5.

The results in Table 5 indicate that when the West Runway and East Runway at ZUTF are operated in an independent parallel departure mode with a reduced divergence angle from 14 degree to 10°, the probability of aircraft collision risk is all less than the overall safety target level (1.0×10^{-8}). Therefore, it is considered that the operation spacing for the departing aircraft is safe and that the divergence angle for the simultaneous use of the two long-distance West Runway and East Runway at ZUTF can be reduced to 10°.

4.2. V-Open Multirunway Capacity Evaluation

4.2.1. Theoretical Analysis. When the departing aircraft on the East Runway has a divergence angle of 15°, the aircraft departure protection area is 724 m from the North Runway. Therefore, the aircraft on the East Runway will affect the departure of aircraft on the North Runway.

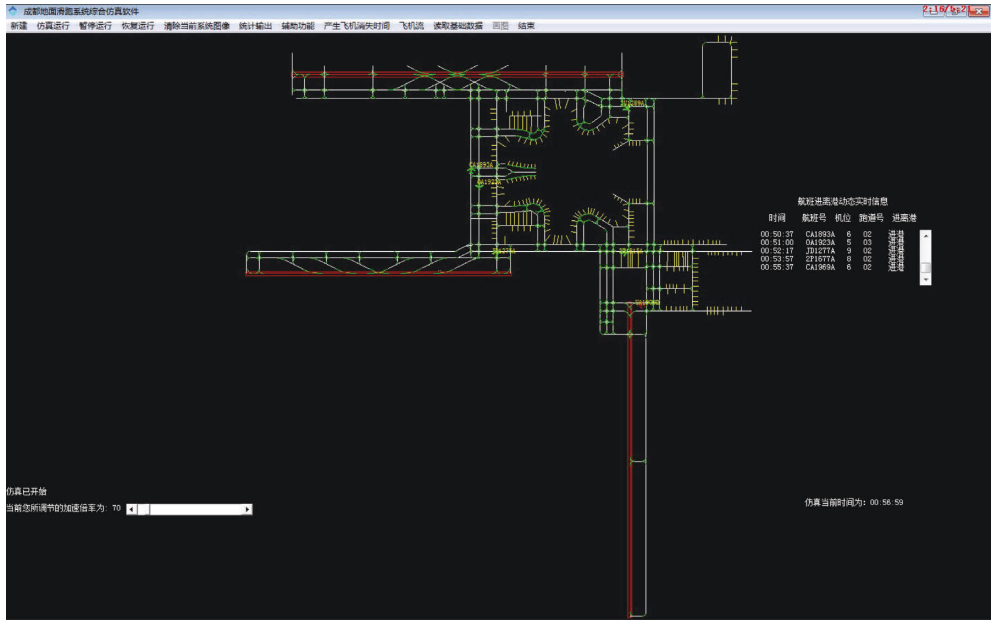

Figure 8: Ground simulation interface.

After the aircraft on the North Runway has taxied for $t_h = 25s$, the air traffic controller can allow the release of the departing aircraft on the East Runway. The departing aircraft on the East Runway is released at $t_z = 70s$, and the departing aircraft on the North Runway can then be aligned to the runway and allowed to taxi.

When applying the ELSO standard, the departure divergence angle is reduced to 10°. In this case, the departure protection zone of the departing aircraft on the East Runway still overlaps with the head of the North Runway, but the overlap distance is reduced to 494 m. Because departing aircraft on the North Runway have a taxiing distance of 600 m behind the runway head, the departing aircraft on East Runway are not limited by the divergence angle of 10°.

The improvements in the runway capacity when using the proposed model and associated parameters are given in Table 6. The capacity results for the conventional standard (divergence angle of 15°) and the ELSO standard (divergence angle of 10°) are presented in Table 7. It is clear that the number of flights per hour can increase by six with the reduced divergence angle.

4.2.2. Simulation Results. In order to test the theoretical results, several simulation experiments were performed for ZUTF based on the general airport simulation software jointly developed using the Visual Basic programming language. This airport surface simulation software has been approved by the ATC office of the CAAC. The airport runway layout was first set to summarize the measurement data of the airport ground flight area, and AutoCAD software was used to build a ground simulation model. After standardizing the positioning point information, two-dimensional coordinate information, taxi-path constraint rules, and parking space information, these data were imported into the ground capacity evaluation system to establish the ground simulation capacity evaluation model at ZUTF. The simulation interface is shown in Figure 8.

In accordance with the regulations for ZUTF operation, the North Runway, East Runway, and West Runway account for 70%, 5%, and 25%, respectively, of all departing flights, while the East Runway and West Runway account for 83% and 17%, respectively, of all arriving flights.

The flight schedule is selected as the data source of the simulation evaluation model, and the ground parameters used in the simulation program are listed in Table 8. Considering the characteristics of runway operation and operating rules, and under the restriction conditions of the percentages of the numbers of arriving and departing flights, the flight flow distribution proportion for each hour, and other characteristics, the original flight schedule of a typical day was randomly selected to generate pressurized flight and aircraft flows for use in the simulations.

Table 9 presents the results from the simulations of the air-ground joint operation capacity of the runway system at ZUTF under the conventional standard (divergence angle of 15°) and the ELSO standard (divergence angle of 10°). The runway capacity under the conventional standard was 74 per hour, which is less than that under the proposed ELSO standard (81 per hour). There were 8.1% more departing flights for the proposed policy during the peak hour and 11.1% more during the peak quarter than the conventional one. Moreover, the average flight delay time reduced significantly by 30% when using the proposed policy. Furthermore, given that 95% of flights involved medium aircraft and 5% involved heavy aircraft with an average passenger load factor of 85%, it can be inferred that passenger turnover at ZUTF would increase by about 6.3%.

The present theoretical analysis and simulations have demonstrated that the efficiency of ZUTF can be markedly

Table 8: Simulation operating parameters.

Simulation parameter	Value
Takeoff runway occupation time	50 s
Landing runway occupation time (fast departure lane)	50 s
Landing runway occupation time (end of runway)	75 s
Minimum time interval between consecutive takeoffs	100 s
Minimum time interval for continuous landings	100 s
Minimum distance between the landing aircraft and the entrance required to issue the takeoff permission	95 s
Time to cross the taxiway starting from standstill	40 s
Runway threshold speed	150 kt
Rapid departure speed	30 kt
Main slide and vertical connecting track speed	20 kt
General taxiway speed	10 kt
Taxi speed in apron area	5 kt
Time from the sliding position withdrawing the wheel to the completion of driving	150 s

Table 9: Simulation results under the conventional standard and the ELSO standard.

Operation mode	Flight number in peak hour	Total flight number	Average delay (min)	Delay in the air (min)	Delay on the ground (min)	Peak hour delay (min)	Flight number in peak quarter
Conventional standard	74	1189	7.9	4.2	4.7	13.9	18
ELSO standard	81	1264	6.8	3.0	3.8	13.6	20
Improvement	+8.1%	+6.3%	−13.9%	−30%	−19%	+2.1%	+11.1%

improved when the divergence angle of aircraft on the East Runway is reduced from 15° to 10°. This results in no overlap in the ground starting area, and the departure operations on the two runways are independent of each other. During operations, it is only necessary to consider that the go-around aircraft on the East Runway will release aircraft on the North Runway before 4.2 km from the runway entrance, which can effectively improve runway capacity by about 10%.

In summary, the proposed policy can improve (1) airport capacity for either parallel runways or diverging runways, (2) the travel experience in civil aviation with a higher flight punctuality rate, and (3) airspace resource optimization with more flexible operation procedures. The present research results can provide theoretical guidance for the future development strategies of the CAAC.

5. Conclusion

Limited by the conventional separation standard of 15 degrees, V-open multiple runways cannot perform its maximum operation function. A collision risk model is proposed to assess the feasibility and safety of the proposed policy at ZUTF airport. A novel capacity estimation model for V-open multiple runways is built to test the operating efficiency of the proposed new separation standard relative to the conventional one. Comparative experiments based on actual flight data from Chengdu Tianfu International Airport showed that the probability of aircraft collision risk is all less than the overall safety target level when divergence angle reduced from 15 degree to 10 degree and new capacity model effectively improves runway capacity by about 10%.

The present research findings can provide theoretical guidance for the CAAC to apply an operation standard to future V-open multiple runways. They might also be useful as a reference for capacity evaluations at airports with diverging runways used for civil aviation. In the future, when divergence angle is reducing from 15 degree to 10 degree, the proposed ELSO standard can also be applied in other airports with three parallel runways to improve the efficiency of airspace in China. Furthermore, the trajectories of go-around aircraft could also cover the diverging runway area for independent parallel approaching operation. Therefore, we will attempt to modify our capacity model with such considerations in our future work.

Data Availability

The trajectory data sampled from the Air Traffic Management Bureau, Civil Aviation Administration of China, used to support the findings of this study, are available from the corresponding author upon request.

Conflicts of Interest

The authors declare that there are no conflicts of interest in this paper.

Acknowledgments

The authors acknowledge the financial support from the National Natural Science Foundation of China [grant no. 61773202] and Technology Project of Air Traffic Management, Civil Aviation Administration of China [grant no.TPATM201903].

References

[1] IATA, "IATA forecast Predicts 8.2 billion air Travelers in 2037," IATA, Available at: https://www.iata.org/en/, 2018.

[2] X. Sun, S. Wandelt, and A. Zhang, "Technological and educational challenges towards pandemic-resilient aviation," *Transport Policy*, vol. 114, pp. 104–115, 2021.

[3] H. Xiong, *Research on cross-Runway configuration and Operation mode[D]*, Civil Aviation Flight University of China, Guanghan, 2020.

[4] Civil Aviation Administration of China, *Air Traffic Management Rules of Civil Aviation Administration of China, CCAR-93TM-R5[S]*, Civil Aviation Administration of China, Beijing, 2009.

[5] Parallel Runway Simultaneous, *Parallel Runway Simultaneous Instrument Operation Management Regulations*, Decree of CAAC NO.123, Beijing, 2004.

[6] M. Cheng, Y. Li, and X. Han, "Constructing Scenarios' Network-of-flight conflict in approach of intersecting runway," *Journal of Advanced Transportation*, vol. 2021, no. 6, pp. 1–11, 2021.

[7] A. D. Mundra, H. Bateman, and A. P. Smith, "Converging runway Display Aid in the NAS: challenges, successes and outlook[C]," in *Proceedings of the 2011 IEEE/AIAA 30th Digital Avionics Systems Conference*, IEEE, Seattle, WA, USA, October 2011.

[8] X. Zhou, D. Zhu, and C. Li, "Optimization of MACAD model for intersecting runway capacity estimation[J]," *Aeronautical Computing Technique*, vol. 48, no. 3, pp. 91–94, 2018.

[9] S. Wang, Y. Zhang, H. Yu, and P. Wen, "A fast method to evaluate the runway capacity at the airport based on arrival/departure capacity curve," in *Proceedings of the Automation and Logistics (ICAL)*, IEEE, Chongqing, China, August 2011.

[10] C. Xu and L. Xin, "Cross-runway collision risk assessment under different crossing angles[J]," *Aeronautical Computing Technology*, vol. 48, no. 01, pp. 74–78, 2018.

[11] R. H. Mayer, D. J. Zondervan, and A. A. Herndon, "A standard for equivalent lateral spacing operations–parallel and reduced divergence departures[C]," in *Proceedings of the Ninth USA/EUROPE Air Traffic Management Research and Development Seminar (ATM2011)*, Berlin, Germany, 2011.

[12] S. Neyshabouri and L. Sherry, "Analysis of airport surface operations: a case-study of Atlanta Hartfield airport," in *Proceedings of the Transportation Research Board 93rd Annual Meeting*, pp. 12–16, Washington, DC, USA, 2014.

[13] Federal Aviation Administration, *D10 TRACON Order D10 7110..65, D10 TRACON Air Traffic Control*, Dallas/Fort Worth, TX, 2010.

[14] Y. Li, "Organizational and interorganizational factors affecting safety in the Chinese civil aviation industry," *Social Behavior and Personality: an International Journal*, vol. 47, no. 5, pp. 1–7, 2019.

[15] X. Qiu, "Development in Chinese transportation construction [M]," in *China 40 Years Infrastructure Construction*, pp. 79–98, Springer, Singapore, 2020.

[16] D. Xue, Z. Liu, B. Wang, and J Yang, "Impacts of COVID-19 on aircraft usage and fuel consumption: a case study on four Chinese international airports," *Journal of Air Transport Management*, vol. 95, Article ID 102106, 2021.

[17] D. Guo and D. Huang, "PBN operation advantage analysis over conventional navigation[J]," *Aerospace Systems*, vol. 4, no. 4, pp. 335–343, 2021.

[18] K. R. Sprong, B. M. Haltli, and J. S. DeArmon, "Improving flight efficiency through terminal area RNAV[C]," in *Proceedings of the 6th USA/Europe Air Traffic Management R&D Seminar*, 2005.

[19] X. Zhou, D. Zhu, C. Li, and Ti Wu, "Optimization of MACAD runway capacity evaluation model under cross-runway configuration[J]," *Aeronautical Computing Technology*, vol. 48, no. 03, pp. 91–94, 2018.

[20] T. M. Cheung, "The Riddle in the Middle: China's central military commission in the Twenty-first Century[M]," in *Influence on China's National Security Policymaking*, pp. 84–119, Stanford University Press, 2020.

[21] M. E. Johnson, X. Zhao, B. Faulkner, and J. P Young, "Statistical models of runway Incursions based on runway intersections and Taxiways," *Journal of Aviation Technology and Engineering*, vol. 5, no. 2, p. 3, 2016.

[22] Y. S. Ebrahimi and K. S. Chun, *Parallel Runway Requirement Analysis Study*, NASA, 1993.

[23] Y. Y. Tee and Z. W. Zhong, "Modelling and simulation studies of the runway capacity of Changi Airport," *Aeronautical Journal*, vol. 122, no. 1253, pp. 1022–1037, 2018.

[24] M. Villegas Díaz, F. Gómez Comendador, J. García-Heras Carretero, and R. M Arnaldo Valdes, "Analyzing the departure runway capacity effects of integrating optimized continuous Climb operations," *International Journal of Aerospace Engineering*, vol. 2019, pp. 1–10, 2019.

[25] J. Lei, X. Chong, D. Chen, Z. Chen, and Q. Chen, "A review of airport runway capacity evaluation model[C]//IOP Conference Series: Materials Science and Engineering," *IOP Conference Series: Materials Science and Engineering*, vol. 780, no. 7, Article ID 072019, 2020.

[26] P. D. Mascio, G. Rappoli, and L. Moretti, "Analytical method for calculating Sustainable airport capacity," *Sustainability*, vol. 12, no. 21, p. 9239, 2020.

[27] Z. Zhang, C. Xu, and T. Lu, "Research on the protection area of lateral runway approach based on radar data[J]," *Journal of Safety and Environment*, vol. 20, no. 4, pp. 1391–1396, 2020.